CLUSTERED HIERARCHICAL ANOMALY AND OUTLIER DETECTION ALGORITHMS

A PREPRINT

Najib Ishaq

Department of Computer Science and Statistics University of Rhode Island Kingston, RI najib_ishaq@uri.edu

Thomas J. Howard III

Department of Computer Science and Statistics University of Rhode Island Kingston, RI thoward27@uri.edu

Noah M. Daniels

Department of Computer Science and Statistics
University of Rhode Island
Kingston, RI
noah_daniels@uri.edu

March 7, 2022

ABSTRACT

Anomaly and outlier detection in datasets is a long-standing problem in machine learning. In some cases, anomaly detection is easy, such as when data are drawn from well-characterized distributions such as the Gaussian. However, when data occupy high-dimensional spaces, anomaly detection becomes more difficult. We present CLAM (Clustered Learning of Approximate Manifolds), a fast hierarchical clustering technique that learns a manifold in a Banach space defined by a distance metric. CLAM induces a graph from the cluster tree, based on overlapping clusters determined by several geometric and topological features. On these graphs, we implement CHAODA (Clustered Hierarchical Anomaly and Outlier Detection Algorithms), exploring various properties of the graphs and their constituent clusters to compute scores of anomalousness. On 24 publicly available datasets, we compare the performance of CHAODA (by measure of ROC AUC) to a variety of state-of-the-art unsupervised anomaly-detection algorithms. Six of the datasets are used for training. CHAODA outperforms other approaches on 14 of the remaining 18 datasets.

1 Introduction

Detecting anomalies and outliers from data is a well-studied problem in machine learning. When data occupy easily-characterizable distributions, such as the Gaussian, the task is relatively easy: one need only identify when a datum is sufficiently far from the mean. However, in "big data" scenarios, where data can occupy high-dimensional spaces, anomalous behavior becomes harder to quantify. If the data happen to be uniformly distributed, one can conceive of simple mechanisms, such as a one-class SVM, that would be effective in any number of dimensions. However, real-world data are rarely distributed uniformly. Instead, data often obey the "manifold hypothesis" [10], occupying a low-dimensional manifold in a high-dimensional embedding space, similar to how a 2-d sheet of paper, once crumpled, occupies a 3-dimensional space. Detecting anomalies in such a landscape is not easy. Imagine trying to identify if a point within the sphere of crumpled paper were anomalous, identifying whether or not the point sits on the sheet or within a gap of the lower-dimensional manifold presents a challenge.

Anomalies (data that do not belong to a distribution) and outliers (data which represent the extrema of a distribution) are found in datasets for a variety of reasons. Errors in the measurement of data cause anomalous records to be stored, novel instances of data emerge over time, or normal behavior may evolve towards the outliers. Moreover, even if data

collection is executed perfectly and shifts in behavior are accounted for, there is still the risk of adversarial attacks on machine-learning algorithms causing undesired behavior [8].

Modern algorithms designed to detect anomalous behavior fail for a variety of reasons, in particular when anomalies live close to, but not on, a complex manifold in high-dimensional space. Our approach is designed to map these complex manifolds. Here we briefly survey contemporary approaches to anomaly detection in order to provide the context needed to understand how our approach differs.

1.1 Clustering-based Approaches

Clustering refers to techniques for grouping points in a way that provides value. This is generally done by assigning *similar* points to the same cluster. Given a clustering and a new point, one can estimate the anomalousness of that new point by measuring its distance to its nearest cluster(s).

There have been few advancements in clustering techniques over the past decade [40]. This may be explained by the poor performance, thus far, of clustering in high-dimensional space [43].

Distance-based clustering relies on some distance measure to partition data into several clusters. Within this approach, the numbers or sizes of clusters are often predetermined: either user-specified, or randomly chosen [40]. Examples of distance-based clustering algorithms are K-Means [25], PAM [18], CLARANS [26] and CLARA [18].

Hierarchical clustering methods build a tree, where points are allocated into leaves [40]. These trees can be created via bottom-up (agglomerative) or top-down (divisive) [1] clustering. The high cost of all-pairs distance computations is often a drawback. Examples of hierarchical clustering algorithms include MST [42], CURE [12], and CHAMELEON [17].

Grid-based clustering works via segmenting the entire volume into a discrete number of cells, and then scanning those cells to find regions of high density. The grid structure typically lets these methods scale well to larger datasets. Some examples include STING [41], Wavecluster [37], CLIQUE [1], Clustering Based Local Outlier Factor (CBLOF) [14], and Local Correlation Integral (LOCI) [28].

1.2 Density-based Approaches

Density-based clustering methods rely on finding regions of high point-density separated by regions of lower density. These algorithms generally do not work well when data are sparse or uniformly distributed. Some examples include DBSCAN [9] and DENCLUE [15]. In this paper, we compare against Local Outlier Factor (LOF) [5].

1.3 Graph-based Approaches

Graph-based methods build graph representations of the data by treating points, or collections of points, as nodes in a graph and drawing edges between them based on various rules. In this paper, we compare against Connectivity-based Outlier Factor (COF) [38].

1.4 Distanced-based Approaches

Distance-based methods use direct distance comparisons and largely rely on k-Nearest Neighbors as their substrate [40]. They tend to use the following intuitions. First, points with fewer than p other points within some distance d are outliers; second, the n points with the greatest distances to their k^{th} -nearest neighbor are outliers; and finally, the n points with the greatest average distance to their k nearest neighbors are outliers. We compare against k-Nearest Neighbors (kNN) [31, 32, 2] and Subspace Outlier Detection (SOD) [19].

1.5 Other Approaches

There are several approaches to anomaly detection that do not fall neatly into any of the aforementioned categories. These methods often rely on support vector machines, random forests, or histograms to detect outliers. We compare against seven methods among these: Histogram-Based Outlier Detection (HBOS)[11], Isolation-Forest (IFOREST) [22, 23], One-class Support Vector Machine (OCSVM) [36], Linear Model Deviation-base outlier Detection (LMDD) [3], Lightweight Online Detector of Anomalies (LODA) [30], Minimum Covariance Determinant (MCD) [34, 13], and Subspace Outlier Detection (SOD) [19].

1.6 CHAODA

We introduce a novel technique, Clustered Learning of Approximate Manifolds (CLAM). This approach uses divisive hierarchical clustering to build a map of a manifold in a Banach space [4] defined by a distance metric. The space may also be defined by a distance *function* that does not obey the triangle inequality, though we have not explored what difficulties this might introduce. As the term *manifold learning* has largely become synonymous with dimension reduction for purposes of visualization, we propose *manifold mapping* to refer to approaches that map out properties of the manifold in the original embedding space. Once the manifold has been mapped, it can be used as input for a myriad of anomaly and outlier detection algorithms. We introduce an ensemble of six such algorithms implemented on CLAM: CHAODA (Clustered Hierarchical Anomaly and Outlier Detection Algorithms).

The manifold mapping component is motivated by a hierarchical clustering approach, CHESS [16], designed to accelerate approximate search on large high-dimensional datasets. While CHESS clustered to a specific depth to accelerate search, CLAM divisively clusters the data until each cluster contains only one datum. From this tree, CLAM can induce a graph by mapping clusters to vertices of the graph, and drawing an edge between any two vertices whose corresponding cluster volumes overlap (i.e. the sum of their radii is greater than the distance separating their centers). Clusters can be selected by a fixed depth, or at heterogeneous depths based on geometric properties, such as local fractal dimension, cluster cardinality, or cluster radius. We call graphs constrained to a uniform-depth layer *layer graphs*. We call graphs from heterogeneous depths *optimal graphs*.

Inducing an optimal graph across a variety of depths effectively maps a manifold with a variety of "resolutions". The intuition is that some regions of the manifold may be denser than others, thus, graphs induced from deeper clusters in those regions may be more informative. We can consider clusters at lower depths in the tree to be, in some sense, "lower resolution" than those at greater depth.

Once we have mapped a manifold, we can analyze the cardinality of clusters at different depths, how connected a cluster is, or how often a cluster is visited by random walks on the manifold. These approaches are combined into an ensemble approach to anomaly and outlier detection.

Clustering approaches have suffered from several problems. The most common deficiencies are: ineffective treatment of high dimensionality, the inability to interpret results, and the inability to scale to exponentially-growing datasets [1]. CLAM, as we will demonstrate, largely resolves these issues.

Naïvely, distance-based approaches require either linear time in the size of the data set for each query, or quadratic time to build an index first. CLAM builds an index in expected $\mathcal{O}(n \lg n)$ time, and queries for outlier scores are sub-linear in the size of the dataset.

2 Methods

2.1 CLAM

We present a manifold-mapping algorithm called CLAM (Clustered Learning of Approximate Manifolds). As input, we need a dataset and a distance function for that dataset. A dataset is a collection of n-points in a D-dimensional embedding space, $\mathbf{X} = \{x_1 \dots x_n\}, x_i \in \mathbb{R}^D$. A Distance Function takes two points in the dataset and produces a non-negative real number, $f: (\mathbb{R}^D, \mathbb{R}^D) \mapsto \mathbb{R}^+$. The distance must be such that f(x,x) = 0 and f(x,y) = f(y,x) $\forall x,y \in X$. The distance function may or may not obey the triangle-inequality. In this paper we used L1-norm and L2-norm, which are metrics. We provide proofs of the complexity of each algorithm in the Supplement.

2.1.1 Clustering

We start by building a divisive-hierarchical clustering of the data based on a random sampling of \sqrt{k} points from the k points in a given cluster from the tree. This achieves clustering in expected $\mathcal{O}(n \lg n)$ time, giving us a tree of clusters, with the root containing every point in the dataset and each leaf containing a single point from the dataset. The CLAM clustering algorithm is defined in Algorithm 1. The procedure is inspired from [16], although we have improved upon their partition method. The root-cluster contains all points in the dataset and clusters are recursively partitioned until each leaf-cluster contains only one point.

These clusters have several interesting and important properties for us to consider. These include the *cardinality*, the number of points in a cluster; *center*, the geometric median of points contained in a cluster; *radius*, the distance to the farthest point from the center; and *local fractal dimension*, as described in [16]. We can also consider individual *parent-child ratios* of cardinality, radius, and local fractal dimension, as well as the *exponential moving averages* of those parent-child ratios along a branch of the tree. Each of these properties is computed during the process of

Algorithm 1 Partition

clustering and cached as metadata for each cluster. In particular, we use the parent-child ratios and the exponential moving averages of those ratios to generalize our method from a small set of datasets to a large, distinct set of datasets.

2.1.2 Graphs

Clusters that are close in the embedding space sometimes have overlapping volumes; i.e., the distance between their centers is less than or equal to the sum of their radii. We define a graph G=(V,E) with the selected clusters in one-to-one correspondence to vertices and with an edge between two vertices if and only if their clusters overlap. Note that any given datapoint will be a member of only one cluster at a given depth in the tree, even though it might exist inside other clusters' radii. Thus, the clusters are not necessarily hyperspheres, but rather polytopes akin to a high-dimensional analog of a Voronoi diagram [39]. Figure 1 illustrates how a graph can be induced by clusters as well as their overlaps at different tree depths.

For our purposes, a graph exhibits an important invariant. The clusters corresponding to vertices in the graph collectively contain every point in the dataset. In addition, each point in the dataset is in exactly one cluster in the graph. A corollary to this invariant is that a graph will never contain two vertices such that one vertex corresponds to an ancestor or descendant cluster of another vertex. A graph can be built from clusters at a fixed depth in the cluster-tree (a layer-graph), or from clusters from multiple different depths in the tree (an optimal-graph). In this work we consider the cardinality of a graph to be *vertex cardinality*; i.e., the number of vertices (clusters) in the graph.

2.1.3 The Manifold

According to the "manifold hypothesis" [10], datasets collected from constrained generating processes that are embedded in a high-dimensional space typically only occupy a low-dimensional manifold in that space. The graphs discussed thus far map this low-dimensional manifold in the original embedding space. Different graphs do this at different levels of local or global resolution. Our aim is to build a graph, where different resolutions may be necessary for different regions of the manifold. We can then apply several anomaly detection algorithms to these graphs.

We describe a set of algorithms in Section 2.3. While mainly relying on graph information, these algorithms can also incorporate information from the tree, such as the child-parent cardinality ratio method described in Section 2.3.4. While these algorithms are themselves fairly simple, the real challenge is in selecting the right clusters for the graphs for these algorithms to operate upon. We will demonstrate CLAM's manifold mapping to be effective enough that even these simple algorithms, more often than not, outperform state-of-the-art anomaly detection algorithms.

2.2 Induced Graphs

The heart of the problem with CHAODA is building the right graph(s) to represent the underlying manifold. One could try using every possible combination of clusters to form every possible graph but this leads to combinatorial explosion. Instead, we must intelligently select those clusters that build a graph which performs well for anomaly detection.

Area under the curve (AUC) of the receiver operating characteristic (ROC) is often used to measure the performance of anomaly detectors; we wish to choose clusters that are expected to maximize this measure. We do this by learning a function that takes a cluster and predicts its contribution to the AUC if that cluster were selected for the graph. Any function $f: Cluster \mapsto \mathbb{R}^+$ will suffice. This is essentially transfer learning: we will learn such functions from a set of

datasets *completely distinct from* the set of datasets we use for benchmarking. We are not learning any dataset-specific parameters, but instead the general geometric and topological properties common among datasets.

We choose a linear regression model and a regression tree model to fill this role. Such models require training data. To generate this data, we take a random sample from the datasets described in Section 2.6, choosing six datasets at random with between 1,000 and 100,000 points. We generate CLAM manifolds for these training datasets, use the linear regression and regression tree models to learn from these datasets, and apply the results to an entirely different collection of datasets. The process is as follows.

We generate CLAM trees for each training dataset. We generate the initial training data by considering layer-graphs induced from these trees. For each such graph, we calculate the arithmetic, geometric, and harmonic means of the parent-child cardinality ratio, radius ratio, and local fractal dimension ratio; along with the exponential moving averages of these ratios, as described in Section 2.1.1. Each set of means forms a 6-dimensional feature vector, giving us three feature vectors for each graph. For each individual algorithm described in Section 2.3, we apply it to the graph and obtain an AUC ROC. We then train the linear regression and decision tree models to predict this AUC from the feature vectors extracted from the graph. The result is a set of models for each individual algorithm of CHAODA, trained from the six training datasets; the decision functions from the fitted models are then used to make predictions for all test datasets, regardless of any differences in dimensionality or other properties of those datasets.

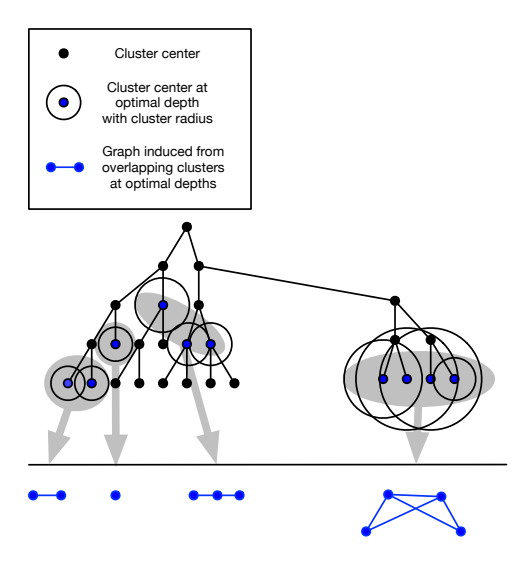


Figure 1: How CLAM induces a graph from a cluster tree. Dots in the tree represent cluster centers; blue dots represent cluster centers chosen as graph vertices. Circles represent the volume of a cluster (the radius is the distance from the center to the furthest point contained within that cluster). Gray arrows point to the induced subgraphs, which are indicated in blue below the horizontal line.

2.3 Individual Algorithms

Here we describe six simple methods for anomaly detection, each of which uses a graph of clusters from CLAM to calculate an anomalousness score for each datapoint. For each algorithm, scores is a dictionary of clusters and their outlier scores, V is the set of clusters in a graph, E is the set of edges in a graph, and the cardinality of a cluster e is denoted by |e|, the number of points in that cluster.

2.3.1 Relative Cluster Cardinality

We measure the anomalousness of a point by the cardinality of the cluster that the point belongs to relative to the cardinalities of the other clusters. Points in the same cluster are considered equally anomalous and points in clusters with lower cardinalities are considered more anomalous than points in clusters with higher cardinalities. The algorithm is defined in Algorithm 2. The time complexity is $\mathcal{O}(|V|)$.

2.3.2 Relative Component Cardinality

We use the usual definition of connected components: no two nodes from different components have an edge between them, and every pair of nodes in the same component has a path connecting them. Consider the relative cardinalities

Algorithm 2 Relative Cluster Cardinality

```
Require: G, a graph
1: for cluster c \in G do
2: scores[c] \leftarrow -|c|
3: end for
```

of each component in much the same way as we considered the relative cardinalities of clusters in the relative cluster cardinality method. Points in clusters (vertices) in smaller components are considered more anomalous than those in larger components, and points in clusters in the same component are considered equally anomalous. The algorithm is defined in Algorithm 3. This algorithm first finds the components of the graph, so its time complexity is $\mathcal{O}(|E| + |V|)$.

Algorithm 3 Relative Component Cardinality

```
Require: G, a graph

1: for component C \in G do

2: scores[C] \leftarrow -|C|

3: end for
```

2.3.3 Graph Neighborhood

Given the graph with clusters and edges, we consider the number of clusters reachable from a starting cluster within a given graph distance k. We call this number the *graph-neighborhood* of the starting cluster. With k small compared to the diameter of the graph, we consider the relative sizes of graph-neighborhoods of the clusters. Points in clusters with small graph-neighborhoods are considered more anomalous than points in clusters with large graph-neighborhoods. The algorithm is defined in Algorithm 4. This algorithm is dominated by computing the eccentricity of each cluster, so its time complexity is $\mathcal{O}(|E| \cdot |V|)$.

Algorithm 4 Graph Neighborhood

```
Require: G, a graph
Require: f \in \mathbb{R} in the range (0,1] (0.25 by default).

1: for cluster c \in G do

2: e_c \leftarrow the eccentricity of c

3: s \leftarrow e_c \cdot f

4: perform a breadth-first traversal from c with s steps

5: v \leftarrow the number of unique clusters visited by the traversal

6: scores[c] \leftarrow -v

7: end for
```

2.3.4 Child-Parent Cardinality Ratio

As described in Section 2.1.1, the partition algorithm used in clustering splits a cluster into two children. If a child cluster contains only a small fraction of its parent's points (thus, the other child has the majority), then we consider the points in that first child cluster to be more anomalous. These child-parent cardinality ratios are accumulated for each point down its branch in the tree, terminating when the child cluster is a node in the induced graph. Points with a low value of these accumulated ratios are considered more anomalous than points with a higher value. The algorithm is defined in Algorithm 5. Unlike other CHAODA algorithms, this one accumulates parent scores into the children. The time complexity of calculating the ratios is $\mathcal{O}(|V|)$ at clustering time, which is amortized over scoring the points; the time complexity of scoring a point is $\mathcal{O}(1)$.

2.3.5 Random Walks

We perform long random walks on each component of a graph and count the number of times that each cluster was visited. We consider the relative visitation counts among the clusters to be inversely related to their anomalousness. The least visited clusters are the most anomalous, and the most visited clusters are the least anomalous. The algorithm is defined in Algorithm 6. This algorithm is dominated by the computation of the transition matrix for the graph. Its worst-case time complexity is $\mathcal{O}(|V|^2)$, but is often better because the transition matrix is computed separately for each component in the graph.

Algorithm 5 Child-Parent Cardinality Ratio

```
Require: G, a graph

1: for cluster c \in G do

2: p \leftarrow the parent cluster of c

3: scores[c] \leftarrow \frac{|p|}{|c|} + scores[p]

4: end for
```

Algorithm 6 Random Walks

```
Require: G = (V, E), a graph
 1: Initialize v[c] \leftarrow 0 \ \forall c \in G
 2: for cluster c \in G do
       c' \leftarrow c
 3:
       for i = 1 to 10 \cdot |V| do
 4:
          c' \leftarrow n(d), a random neighbor of d
 5:
          increment v[c']
 6:
 7:
       end for
 8: end for
 9: for cluster c \in G do
       scores[c] \leftarrow -v[c]
10:
11: end for
```

2.3.6 Stationary Probabilities

We compute the transition probability matrix of each component of a graph that contains at least two clusters. We then compute successive squares of this matrix. This process will eventually converge as long as the graph is connected and aperiodic [21]; we find this convergent matrix. We consider the sum of the values along a row to be inversely related to the anomalousness of the respective cluster. The algorithm is defined in Algorithm 7. This algorithm is dominated by the computation of a separate matrix for each component in the graph. Its worst-case time complexity is $\mathcal{O}(|V|^2)$, but is often better in practice.

Algorithm 7 Stationary Probabilities

```
Require: G, a graph
 1: for component C \in G do
       M \leftarrow the transition matrix for C
 3:
       repeat
          M \leftarrow M^2
 4:
       until M converges
 5:
       for cluster c \in C do
 6:
          s \leftarrow \text{the row from } M \text{ corresponding to } c
 7:
           scores[c] \leftarrow -\Sigma(s)
 8:
 9:
       end for
10: end for
```

2.4 Normalization

The individual algorithms described in 2.3 produce outlier scores for each cluster, rather than for each point. We remedy this by assigning to each point the score of the cluster to which it belongs. Since our graphs guarantee that each point is in exactly one cluster and that every point from the dataset is accounted for, this assigns an outlier score to each point in a dataset. However, the individual methods still produce scores with a wide range of values. The only common feature among these scores is that low scores correspond to inliers and high scores correspond to outliers. Therefore, we cannot directly compare scores across methods, which is needed for ensemble methods. Thus, we normalize to the range [0,1], using gaussian normalization [20] as defined in Algorithm 8. We include sigmoid and min-max normalization as options in our implementation.

Algorithm 8 Gaussian Normalization

```
Require: X, a dataset
```

Require: S, a set of outlier scores for each point in X

```
1: erf: x \mapsto \frac{2}{\sqrt{\pi}} \int_0^x e^{-u^2} du

2: \mu \leftarrow mean(S)

3: \sigma \leftarrow std(S)

4: for point p \in X do

5: S[p] \leftarrow \frac{1}{2} \left(1 + erf\left(\frac{S[p] - \mu}{\sigma \cdot \sqrt{2}}\right)\right)
```

2.5 Ensemble

Given a dataset and a list of distance functions for the dataset, we start by building a CLAM tree for each distance function on the dataset. We extract the parent-child ratios and the exponential moving averages of those ratios for each cluster in each tree. Given the set of models learned from the training datasets described in Section 2.2, we use each model to rank every cluster, normalized by cardinality. The highest ranked clusters from each tree are then used to build a graph. This gives us one graph for each combination of individual algorithm, meta-ML model, and distance function used. We used the six individual algorithms described in 2.3, three means (arithmetic, geometric, and harmonic), two meta-ML models (linear regression and regression trees), and two distance metrics (L1-norm and L2-norm); thus, we have upto 72 graphs for each dataset.

Each graph is then used with its corresponding individual algorithm to calculate an outlier score for each point in the dataset. These outlier scores are then combined into an ensemble by simply taking the mean of all the scores for each point. We present the AUC scores from this ensemble in Section 3.

2.5.1 A Note on Runtime Performance

During testing, we noticed that even though we often see $|V| \ll n$, where n is the number of points in the dataset and V is the set of vertices in a graph, the more expensive methods from 2.3 were prohibitive. We remedy this by only running the expensive algorithms, i.e. graph neighborhood size, random walks, and stationary probabilities, when $|V| < max(128, \lfloor \sqrt{n} \rfloor)$. We compared the effect on AUC of using this threshold and present the results in Table 1 under the CHAODA-fast and CHAODA rows. CHAODA-fast exhibits comparable accuracy to CHAODA, so we set CHAODA-fast as the default in our implementation.

2.6 Datasets

We sourced 24 datasets from Outlier Detection Datasets (ODDS) [33], for training CHAODA and testing its performance. All of these datasets were adapted from the UCI Machine Learning Repository (UCIMLR) [7], and were standardized by ODDS for benchmarks on anomaly and outlier detection.

Of these 24 datasets, we selected six at random for training CHAODA: annthyroid, mnist, pendigits, satellite, shuttle, and thyroid. The remaining datasets were used to benchmark the performance of CHAODA. We benchmarked CHAODA 30 times with the same split of test and training datasets, with different random seeds for CLAM clustering and CHAODA's random walk algorithm. We provide more details on the datasets, including size, dimensionality, and fraction of outliers, in the Supplement. All benchmarks were conducted on a 28-core Intel Xeon E5-2690 v4 2.60GHz, 512GB RAM and CentOS 7 Linux with kernel 3.10.0-1127.13.1.el7.x86_64 #1 SMP and Python 3.6.8.

Note that CHAODA is an unsupervised algorithm. As such, we compare only against other unsupervised algorithms. We compared against 18 unsupervised algorithms collected in the pyOD suite [44] and Scikit-Learn [29], as well as RS-Hash [35]. A supervised version of CHAODA is possible future work which we will compare against supervised methods such as REPEN [27].

3 Results

The performance on the 18 test datasets is in Table 1. Performance on the 6 training datasets is shown in the Supplement. Each column shows the AUC ROC scores of CHAODA and every competitor. The best; i.e., highest, score, and every score within 0.02 of that best score, are presented in bold. In our 30 experimental runs, setting a different random seed resulted in a variance of at most 0.02 AUC.

Table 1: Performance (AUC) of CHAODA vs. other methods on the 18 test datasets.

| MODEL | ARRH | BREASTW | CARDIO | COVER | GLASS | Нттр | Iono. | Lумрно | Маммо |
|----------------------------------|----------------------|----------------------|----------------------|----------------------|---------------------------|-----------------------------|----------------------|----------------------|----------------------|
| CHAODA-FAST | 0.77 | 0.97 | 0.81 | 0.71 | 0.70 | 1.00 | 0.88 | 0.98 | 0.85 |
| CHAODA | 0.75 | 0.97 | 0.80 | 0.75 | 0.70 | 1.00 | 0.88 | 0.98 | 0.86 |
| ABOD | 0.62 | 0.50 | 0.49 | 0.51 | 0.53 | 0.50 | 0.85 | 0.80 | 0.50 |
| AUTOENCODER | 0.65 | 0.91 | 0.74 | 0.52 | 0.54 | 0.51 | 0.65 | 0.83 | 0.51 |
| CBLOF | 0.70 | 0.83 | 0.57 | EX | 0.54 | EX | 0.86 | 0.83 | 0.50 |
| COF | 0.65 | 0.26 | 0.50 | 0.50 | 0.59 | 0.51 | 0.81 | 0.83 | 0.51 |
| HBOS | 0.65 | 0.93 | 0.58 | 0.49 | 0.48 | 0.51 | 0.36 | 0.91 | 0.50 |
| IFOREST | 0.72 | 0.91 | 0.69 | 0.50 | 0.54 | 0.53 | 0.77 | 0.83 | 0.59 |
| KNN | 0.68 | 0.84 | 0.51 | 0.51 | 0.54 | 0.51 | 0.90 | 0.83 | 0.51 |
| LMDD | 0.68 | 0.64 | 0.60 | 0.49 | 0.54 | 0.51 | 0.67 | 0.65 | 0.56 |
| LOCI | 0.62 | TO | TO | TO | 0.58 | TO | 0.58 | 0.90 | TO |
| LODA | 0.65 | 0.93 | 0.60 | 0.52 | 0.48 | 0.51 | 0.63 | 0.48 | 0.52 |
| LOF | 0.67 | 0.30 | 0.49 | 0.50 | 0.54 | 0.51 | 0.79 | 0.83 | 0.53 |
| MCD | 0.65 | 0.94 | 0.55 | 0.50 | 0.48 | 0.50 | 0.90 | 0.83 | 0.51 |
| MOGAAL | 0.42 | 0.40 | 0.45 | TO | 0.59 | TO | 0.36 | 0.48 | TO |
| OCSVM | 0.70 | 0.77 | 0.70 | 0.56 | 0.54 | 0.50 | 0.68 | 0.83 | 0.60 |
| SOD | 0.59 | 0.77 | 0.48 | TO | 0.54 | TO | 0.84 | 0.65 | 0.51 |
| SOGAAL | 0.48 | 0.30 | 0.45 | 0.61 | 0.59 | 0.51 | 0.36 | 0.48 | 0.50 |
| SOS | 0.51 | 0.50 | 0.50 | TO | 0.48 | TO | 0.72 | 0.48 | TO |
| VAE | 0.65 | 0.95 | 0.74 | 0.52 | 0.48 | 0.51 | 0.65 | 0.83 | 0.56 |
| MODEL | Musk | OPTDIGITS | PIMA | SATIMG-2 | SMTP | VERT | VOWELS | WBC | WINE |
| CHAODA-FAST | 1.00 | 0.96 | 0.63 | 1.00 | 0.92 | 0.29 | 0.71 | 0.97 | 0.99 |
| CHAODA | 1.00 | 0.93 | 0.63 | 1.00 | 0.95 | 0.29 | 0.70 | 0.97 | 0.99 |
| ABOD | 0.47 | 0.54 | 0.60 | 0.53 | 0.50 | 0.49 | 0.75 | 0.50 | 0.43 |
| AUTOENCODER | 0.63 | 0.48 | 0.57 | 0.71 | 0.50 | 0.49 | 0.51 | 0.77 | 0.51 |
| CBLOF | 1.00 | 0.52 | 0.64 | 0.90 | 0.50 | 0.49 | 0.52 | 0.82 | 0.46 |
| COF | 0.53 | 0.52 | 0.54 | 0.56 | 0.50 | 0.51 | 0.71 | 0.47 | 0.46 |
| HBOS | 1.00 | 0.60 | 0.55 | 0.49 | 0.68 | 0.47 | 0.56 | 0.77 | 0.57 |
| IFOREST | 0.97 | 0.50 | 0.65 | 0.94 | 0.50 | 0.45 | 0.63 | 0.72 | 0.51 |
| KNN | 0.51 | 0.51 | 0.60 | 0.61 | 0.53 | 0.47 | 0.72 | 0.51 | 0.47 |
| LMDD | 0.48 | 0.49 | 0.37 | 0.49 | 0.65 | 0.43 | 0.49 | 0.80 | 0.62 |
| LOCI | TO | TO | TO | TO | TO | 0.49 | TO | 0.72 | 0.46 |
| LODA | 0.54 | 0.51 | 0.62 | 0.69 | 0.57 | 0.43 | 0.51 | 0.82 | 0.57 |
| LOF | 0.50 | 0.53 | 0.55 | 0.55 | 0.50 | 0.49 | 0.69 | 0.50 | 0.46 |
| MCD | 0.97 | 0.48 | 0.66 | 0.61 | 0.50 | 0.45 | 0.63 | 0.60 | 0.46 |
| | | | | 0.49 | TO | 0.51 | 0.48 | 0.60 | 0.46 |
| MOGAAL | 0.48 | 0.48 | 0.61 | | | | | | |
| MOGAAL OCSVM | 0.48 | 0.49 | 0.56 | 0.84 | 0.50 | 0.49 | 0.50 | 0.82 | 0.46 |
| MOGAAL OCSVM SOD | 0.48 0.51 | 0.49 0.51 | 0.56 0.56 | 0.84 0.58 | 0.50 TO | 0.49 0.45 | 0.50 0.66 | 0.82 0.60 | 0.46 0.46 |
| MOGAAL OCSVM SOD SOGAAL | 0.48 0.51 0.48 | 0.49 0.51 0.52 | 0.56 0.56 0.48 | 0.84 0.58 0.49 | 0.50 <i>TO</i> 0.62 | 0.49 0.45 0.54 | 0.50 0.66 0.48 | 0.82 0.60 0.47 | 0.46 0.46 0.46 |
| MOGAAL OCSVM SOD | 0.48 0.51 | 0.49 0.51 | 0.56 0.56 | 0.84 0.58 | 0.50 TO | 0.49 0.45 | 0.50 0.66 | 0.82 0.60 | 0.46 0.46 |

If a method exceeded 10 hours on a dataset, we terminated it and marked the corresponding cell with "TO". If a method crashed, we mark the cell with "EX". Notably, CHAODA performed best (or tied for best) on 14 of the 18 test datasets. Runtime performance is presented in the Supplement due to space constraints. Note that we implemented CLAM and CHAODA entirely in Python. While we used the provided wrappers for each method we compared against, those methods are often implemented in C/C++. Therefore, the comparison of wall-clock time is not truly fair to CHAODA. A reimplementation in a high-performance language, such as Rust, would be worthwhile.

We considered several recently published algorithms against which to compare. Those with available implementations are included in Table 1. Where we were unable to find a working implementation, we include here the performance claimed by the respective authors. RS-Hash [35] reported AUCs of 0.92 on Cardio, 1.00 on Lympho, 0.99 on Musk, and 0.76 on OptDigits. This beats CHAODA on Cardio, ties on Lympho and Musk, and is outperformed by CHAODA on OptDigits. We considered Clustering with Outlier Removal [24] but we could not find a working implementation and the authors did not report AUC scores, instead only reporting F-measure.

4 Discussion

We have presented CHAODA, an ensemble of six algorithms that use the map of the underlying manifold produced by CLAM. The six individual algorithms are simple to implement on top of CLAM and, when combined into an ensemble, often outperform state-of-the-art methods.

CLAM uses the geometric and topological properties of fractal dimension and metric entropy of the data to build a map of the low-dimensional manifold that the data occupy. CLAM is inspired by the clustering algorithm from CHESS [16] but differs by the introduction a novel graph-induction approach and a notion of optimal depths, learned via a form of "meta-machine-learning" and transfer learning. CLAM's selection of "poles" for partitioning clusters is also more efficient than CHESS. CHAODA builds on this manifold-mapping framework for anomaly and outlier detection. Intuitively, we expect CHAODA to perform particularly well when the data lie on an "interesting" manifold, and to perform merely average when the data derive from an easily-described distribution (or "boring" manifold). Just as CHESS demonstrated an acceleration of search when the data exhibited *low fractal dimension* and *low metric entropy*, with CHAODA, we see that AUC scores are vastly improved when the data exhibit these properties and often competitive when the data do not exhibit these properties. We believe that CLAM is free of hyperparameters; the weights learned from the meta-ML step could vary, but we learned them once on a distinct training set.

We should note the Vertebral Column (Vert.) dataset. Most tested algorithms perform similarly to random guessing, while CHAODA performs much worse. We suspect this is due to how this specific dataset was collected. Each instance represents six biomechanical attributes derived from scans of a patient's pelvis and lumbar spine. This dataset contains 210 instances of the Abnormal class treated as inliers and 30 instances of the Normal class treated as outliers. Each attribute has a narrow range to be in the Normal class but can have a wider range in the Abnormal class. This causes the Normal instances to group together, while Abnormal instances remain distant from each other. Since CHAODA relies on clusters as the substrate, it assigns low scores to instances in the Normal class, i.e. the outliers, and high scores to those in the Abnormal class, i.e. the inliers. Put plainly, CHAODA sees the manifold as the Normal class, which the dataset labels as outliers. This curiosity could be remedied by a supervised version of CHAODA.

The choice of distance function could significantly impact anomaly-detection performance. In this case, domain knowledge is likely the best way to determine the distance function of choice. Future work should explore a more diverse collection of domain-appropriate distance functions, such as Wasserstein distance on images, Levenshtein edit distance on strings, and Jaccard distance on the maximal common subgraph of molecular structures.

CHAODA is demonstrably highly effective on high-dimensional datasets, and so may be applied to neural networks. Using CLAM to map a dataset where each datum represents the activations of a neural network from an input to the neural network, we would expect to detect malicious inputs to neural networks based on the intuition that malicious inputs produce atypical activation patterns.

In conclusion, we have demonstrated that by mapping the manifolds occupied by data, CLAM reveals structure that allows CHAODA to outperform other state-of-the-art approaches to anomaly detection.

References

- [1] AGRAWAL, R., GEHRKE, J., GUNOPULOS, D., AND RAGHAVAN, P. Automatic subspace clustering of high dimensional data for data mining applications. In *Proceedings of the 1998 ACM SIGMOD international conference on Management of data* (1998), pp. 94–105.
- [2] ANGIULLI, F., AND PIZZUTI, C. Fast outlier detection in high dimensional spaces. In *Principles of Data Mining and Knowledge Discovery* (Berlin, Heidelberg, 2002), T. Elomaa, H. Mannila, and H. Toivonen, Eds., Springer Berlin Heidelberg, pp. 15–27.
- [3] ARNING, A., AGRAWAL, R., AND RAGHAVAN, P. A linear method for deviation detection in large databases. In *KDD* (1996), vol. 1141, pp. 972–981.
- [4] BANACH, S. Sur les fonctionnelles linéaires ii. Studia Mathematica 1 (1929), 223–239.
- [5] Breunig, M. M., Kriegel, H.-P., Ng, R. T., and Sander, J. Lof: Identifying density-based local outliers. In *Proceedings of the 2000 ACM SIGMOD International Conference on Management of Data* (New York, NY, USA, 2000), SIGMOD '00, Association for Computing Machinery, p. 93–104.
- [6] COPPERSMITH, D., AND WINOGRAD, S. Matrix multiplication via arithmetic progressions. *Journal of Symbolic Computation* 9, 3 (1990), 251 280. Computational algebraic complexity editorial.
- [7] DUA, D., AND GRAFF, C. UCI machine learning repository, 2017.

- [8] ELSAYED, G., SHANKAR, S., CHEUNG, B., PAPERNOT, N., KURAKIN, A., GOODFELLOW, I., AND SOHL-DICKSTEIN, J. Adversarial examples that fool both computer vision and time-limited humans. In *Advances in Neural Information Processing Systems* (2018), pp. 3910–3920.
- [9] ESTER, M., KRIEGEL, H.-P., SANDER, J., XU, X., ET AL. A density-based algorithm for discovering clusters in large spatial databases with noise. In *Kdd* (1996), vol. 96, pp. 226–231.
- [10] FEFFERMAN, C., MITTER, S., AND NARAYANAN, H. Testing the manifold hypothesis. *Journal of the American Mathematical Society* 29, 4 (2016), 983–1049.
- [11] GOLDSTEIN, M., AND DENGEL, A. Histogram-based outlier score (hbos): A fast unsupervised anomaly detection algorithm. *KI-2012: Poster and Demo Track* (2012), 59–63.
- [12] GUHA, S., RASTOGI, R., AND SHIM, K. Cure: an efficient clustering algorithm for large databases. *ACM Sigmod record* 27, 2 (1998), 73–84.
- [13] HARDIN, J., AND ROCKE, D. Outlier detection in the multiple cluster setting using the minimum covariance determinant estimator. *Computational Statistics and Data Analysis* 44, 4 (Jan. 2004), 625–638.
- [14] HE, Z., XU, X., AND DENG, S. Discovering cluster-based local outliers. *Pattern Recognition Letters* 24, 9 (2003), 1641 1650.
- [15] HINNEBURG, A., KEIM, D. A., ET AL. An efficient approach to clustering in large multimedia databases with noise. In KDD (1998), vol. 98, pp. 58–65.
- [16] ISHAQ, N., STUDENT, G., AND DANIELS, N. M. Clustered hierarchical entropy-scaling search of astronomical and biological data. In 2019 IEEE International Conference on Big Data (Big Data) (2019), IEEE, pp. 780–789.
- [17] KARYPIS, G., HAN, E.-H., AND CHAMELEON, V. K. A hierarchical clustering algorithm using dynamic modeling. *IEEE Computer 32*, 8 (1999), 68–75.
- [18] KAUFMAN, L., AND ROUSSEEUW, P. J. Finding groups in data: an introduction to cluster analysis, vol. 344. John Wiley & Sons, 2009.
- [19] KRIEGEL, H.-P., KRÖGER, P., SCHUBERT, E., AND ZIMEK, A. Outlier detection in axis-parallel subspaces of high dimensional data. In *Advances in Knowledge Discovery and Data Mining* (Berlin, Heidelberg, 2009), T. Theeramunkong, B. Kijsirikul, N. Cercone, and T.-B. Ho, Eds., Springer Berlin Heidelberg, pp. 831–838.
- [20] KRIEGEL, H.-P., KROGER, P., SCHUBERT, E., AND ZIMEK, A. Interpreting and unifying outlier scores. In *Proceedings of the 2011 SIAM International Conference on Data Mining* (2011), SIAM, pp. 13–24.
- [21] LEVIN, D. A., AND PERES, Y. Markov chains and mixing times, vol. 107. American Mathematical Soc., 2017.
- [22] LIU, F. T., TING, K. M., AND ZHOU, Z.-H. Isolation forest. In *Proceedings of the 2008 Eighth IEEE International Conference on Data Mining* (USA, 2008), ICDM '08, IEEE Computer Society, p. 413–422.
- [23] LIU, F. T., TING, K. M., AND ZHOU, Z.-H. Isolation-based anomaly detection. *ACM Trans. Knowl. Discov. Data* 6, 1 (Mar. 2012).
- [24] LIU, H., LI, J., WU, Y., AND FU, Y. Clustering with outlier removal. *IEEE Transactions on Knowledge and Data Engineering* (2019).
- [25] MACQUEEN, J., ET AL. Some methods for classification and analysis of multivariate observations. *Proceedings of the fifth Berkeley symposium on mathematical statistics and probability 1*, 14 (1967), 281–297.
- [26] NG, R., AND HAN, J. Efficient and effective clustering methods for spatial data. In *Proc_of the Int. Conf. on Very Large Data Bases, Santiago, Chile* (1994).
- [27] PANG, G., CAO, L., CHEN, L., AND LIU, H. Learning representations of ultrahigh-dimensional data for random distance-based outlier detection. In *Proceedings of the 24th ACM SIGKDD International Conference on Knowledge Discovery & Data Mining* (2018), pp. 2041–2050.
- [28] PAPADIMITRIOU, S., KITAGAWA, H., GIBBONS, P. B., AND FALOUTSOS, C. Loci: fast outlier detection using the local correlation integral. *Proceedings 19th International Conference on Data Engineering (Cat. No.03CH37405)* (2003), 315–326.
- [29] PEDREGOSA, F., VAROQUAUX, G., GRAMFORT, A., MICHEL, V., THIRION, B., GRISEL, O., BLONDEL, M., PRETTENHOFER, P., WEISS, R., DUBOURG, V., ET AL. Scikit-learn: Machine learning in python. *the Journal of machine Learning research* 12 (2011), 2825–2830.
- [30] PEVNÝ, T. Loda: Lightweight on-line detector of anomalies. Machine Learning 102, 2 (Feb 2016), 275–304.
- [31] RAMASWAMY, S., RASTOGI, R., AND SHIM, K. Efficient algorithms for mining outliers from large data sets. In *Proceedings of the 2000 ACM SIGMOD international conference on Management of data* (2000), pp. 427–438.

- [32] RAMASWAMY, S., RASTOGI, R., AND SHIM, K. Efficient algorithms for mining outliers from large data sets. In *ACM SIGMOD Record* (06 2000), vol. 29, pp. 427–438.
- [33] RAYANA, S. ODDS library, 2016.
- [34] ROUSSEEUW, P., AND DRIESSEN, K. A fast algorithm for the minimum covariance determinant estimator. *Technometrics* 41 (08 1999), 212–223.
- [35] SATHE, S., AND AGGARWAL, C. C. Subspace outlier detection in linear time with randomized hashing. In 2016 IEEE 16th International Conference on Data Mining (ICDM) (2016), IEEE, pp. 459–468.
- [36] SCHÖLKOPF, B., PLATT, J. C., SHAWE-TAYLOR, J., SMOLA, A. J., AND WILLIAMSON, R. C. Estimating the support of a high-dimensional distribution. *Neural Computation* 13, 7 (2001), 1443–1471.
- [37] SHEIKHOLESLAMI, G., CHATTERJEE, S., AND ZHANG, A. Wavecluster: a wavelet-based clustering approach for spatial data in very large databases. *The VLDB Journal* 8, 3-4 (2000), 289–304.
- [38] TANG, J., CHEN, Z., FU, A. W.-C., AND CHEUNG, D. W.-L. Enhancing effectiveness of outlier detections for low density patterns. In *Proceedings of the 6th Pacific-Asia Conference on Advances in Knowledge Discovery and Data Mining* (Berlin, Heidelberg, 2002), PAKDD '02, Springer-Verlag, p. 535–548.
- [39] VORONOI, G. Nouvelles applications des paramètres continus à la théorie des formes quadratiques. premier mémoire. sur quelques propriétés des formes quadratiques positives parfaites. *Journal für die reine und angewandte Mathematik 1908*, 133 (1908), 97–102.
- [40] WANG, H., BAH, M. J., AND HAMMAD, M. Progress in outlier detection techniques: A survey. *IEEE Access* 7 (2019), 107964–108000.
- [41] WANG, W., YANG, J., MUNTZ, R., ET AL. Sting: A statistical information grid approach to spatial data mining. In *VLDB* (1997), vol. 97, pp. 186–195.
- [42] ZAHN, C. T. Graph-theoretical methods for detecting and describing gestalt clusters. *IEEE Transactions on computers* 100, 1 (1971), 68–86.
- [43] ZHANG, J. Advancements of outlier detection: A survey. *ICST Transactions on Scalable Information Systems 13*, 1 (2013), 1–26.
- [44] ZHAO, Y., NASRULLAH, Z., AND LI, Z. Pyod: A python toolbox for scalable outlier detection. *Journal of Machine Learning Research* 20, 96 (2019), 1–7.

5 Datasets

Here we describe the datasets we use for benchmarks. See Table S2 for a summary of this information.

The **annthyroid** dataset is derived from the "Thyroid Disease" dataset from the UCIMLR. The original data has 7200 instances with 15 categorical attributes and 6 real-valued attributes. The class labels are "normal", "hypothyroid", and "subnormal" classes are combined into 534 outlier instances, and only the 6 real-valued attributes are used.

The **arrhythmia** dataset is derived from the "Arrhythmia" dataset from the UCIMLR. The original dataset contains 452 instances with 279 attributes. There are five categorical attributes which are discarded, leaving this as a 274-dimensional dataset. The instances are divided into 16 classes. The eight smallest classes collectively contain 66 instances and are combined into the outlier class.

The **breastw** dataset is also derived from the "Breast Cancer Wisconsin (Original)" dataset. This is a 9-dimensional dataset containing 683 instances of which 239 represent malignant tumors and are treated as the outlier class.

The **cardio** dataset is derived from the "Cardiotocography" dataset. The dataset is composed of measurements of fetal heart rate and uterine contraction features on cardiotocograms. The are each labeled "normal", "suspect", and "pathologic" by expert obstetricians. For anomaly detection, the "normal" class forms the inliers, the "suspect" class is discarded, and the "pathologic" class is downsampled to 176 instances forming the outliers. This leaves us with 1831 instances with 21 attributes in the dataset.

The **cover** dataset is derived from the "Covertype" dataset. The original dataset contains 581,012 instances with 54 attributes. The dataset is used to predict the type of forest cover solely from cartographic variables. The instances are labeled into seven different classes. For outlier detection, we use only the 10 quantitative attributes as the features. We treat class 2 (lodgepole pine) as the inliers, and class 4 (cottonwood/willow) as the outliers. The remaining classes are discarded. This leaves us with a 10-dimensional dataset with 286,048 instances of which 2,747 are outliers.

The **glass** dataset is derived from the "Glass Identification" dataset. The study of classification of types of glass was motivated by criminological investigations where glass fragments left at crime scenes were used as evidence. This dataset contains 214 instances with 9 attributes. While there are several different types of glass in this dataset, class 6 is a clear minority with only 9 instances and, as such, points in class 6 are treated as the outliers while all other classes are treated as inliers.

The **http** dataset is derived from the original "KDD Cup 1999" dataset. It contains 41 attributes (34 continuous and 7 categorical) which are reduced to 4 attributes (service, duration, src_bytes, dst_bytes). Only the "service" attribute is categorical, dividing the data into {http, smtp, ftp, ftp_data, others} subsets. Here, only the "http" data is used. The values of the continuous attributes are centered around 0, so they have been log-transformed far away from 0. The original data contains 3,925,651 attacks in 4,898,431 records. This smaller dataset is created with only 2,211 attacks in 567,479 records.

The **ionosphere** dataset is derived from the "Ionosphere" dataset. It consists of 351 instances with 34 attributes. One of the attributes is always 0 and, so, is discarded, leaving us with a 33-dimensional dataset. The data come from radar measurements of the ionosphere from a system located in Goose Bay, Labrador. The data are classified into "good" if the radar returns evidence of some type of structure in the ionosphere, and "bad" otherwise. The "good" class serves as the inliers and the "bad" class serves as the outliers.

The **lympho** dataset is derived from the "Lymphography" dataset. The data contain 148 instances with 18 attributes. The instances are labeled "normal find", "metastases", "malign lymph", and "fibrosis". The two minority classes only contain a total of six instances, and are combined to form the outliers. The remaining 142 instances form the inliers.

The **mammography** dataset is derived from the original "Mammography" dataset provided by Aleksandar Lazarevic. Its goal is to use x-ray images of human breasts to find calcified tissue as an early sign of breast cancer. As such, the "calcification" class is considered as the outlier class while the "non-calcification" class is the inliers. We have 11,183 instances with 6 attributes, of which 260 are "calcifications."

The **mnist** dataset is derived from the classic "MNIST" dataset of handwritten digits. Digit-zero is considered the inlier class while 700 images of digit-six are the outliers. Furthermore, 100 pixels are randomly selected as features from the original 784 pixels.

The **musk** dataset is derived from its namesake in the UCIMLR. It is created from molecules that have been classified by experts as "musk" or "non-musk". The data are downsampled to 3,062 instances with 166 attributes. The "musk" class forms the outliers while the "non-musk" class forms the inliers.

The **optdigits** dataset is derived from the "Optical Recognition of Handwritten Digits" dataset. Digits 1–9 form the inliers while 150 samples of digit-zero form the outliers. This gives us a dataset of 5,216 instances with 64 attributes.

The **pendigits** dataset is derived from the "Pen-Based Recognition of Handwritten Digits" dataset from the UCI Machine Learning Repository. The original collection of handwritten samples is reduced to 6,870 points, of which 156 are outliers.

The **pima** dataset is derived from the "Pima Indians Diabetes" dataset. The original dataset presents a binary classification problem to detect diabetes. This subset was restricted to female patients at least 21 years old of Pima Indian heritage.

The **satellite** dataset is derived from the "Statlog (Landsat Satellite)" dataset. The smallest three classes (2, 4, and 5) are combined to form the outlier class while the other classes are combined to form the inlier class. The train and test subsets are combined to produce a of 6,435 instances with 36 attributes.

The **satimage-2** dataset is also derived from the "Satlog (Landsat Satellite)" dataset. Class 2 is downsampled to 71 instances that are treated as outliers, while all other classes are combined to form an inlier class. This gives us 5,803 instances with 36 attributes.

The **shuttle** dataset is derived from the "Statlog (Shuttle)" dataset. There are seven classes in the original dataset. Here, class 4 is discarded, class 1 is treated as the inliers and the remaining classes, which are comparatively small, are combined into an outlier class. This gives us 49,097 instances with 9 attributes, of which 3,511 are outliers.

The **smtp** is also derived from the "KDD Cup 1999" dataset. It is pre-processed in the same way as the **http** dataset, except that the "smtp" service subset is used. This version of the dataset only contains 95,156 instances with 3 attributes, of which 30 instances are outliers.

The **thyroid** dataset is also derived from the "Thyroid Disease" dataset. The attribute selection is the same as for the **annthyroid** dataset but only the 3,772 training instances are used in this version. The "hyperfunction" class, containing 93 instances, is treated as the outlier class, while the other two classes are combined to form an inlier class.

The **vertebral** dataset is derived from the "Vertebral Column" dataset. 6 attributes are derived to represent the shape and orientation of the pelvis and lumbar spine. These attributes are: pelvic incidence, pelvic tilt, lumbar lordosis angle, sacral slope, pelvic radius and grade of spondylolisthesis. Each instance comes from a different patient. The "Abnormal (AB)" class of 210 instances are used as inliers while the "Normal (NO)" class is downsampled to 30 instances to be used as outliers.

The **vowels** dataset is derived from the "Japanese Vowels" dataset. The UCIMLR presents this data as a multivariate time series of nine speakers uttering two Japanese vowels. For outlier detection, each frame of each time-series is treated as a separate point. There are 12 features associated with each time series, and these translate as the attributes for each point. Data from speaker 1, downsampled to 50 points, form the outlier class. Speakers 6, 7, and 8 form the inlier class. The rest of the points are discarded. This leaves is with 1,456 points in 12 dimensions, of which 50 are outliers.

The **wbc** dataset is derived from the "Wisconsin-Breast Cancer (Diagnostics)" dataset. The dataset records measurements for breast cancer cases. The benign class is treated as the inlier class, while the malignant class is downsampled to 21 points and serves as the outlier class. This leaves us with 278 points in 30 dimensions.

The **wine** dataset is a collection of results of a chemical analysis of several wines from a region in Italy. The data contain 129 samples having 13 attributes, and divided into 3 classes. Classes 2 and 3 form the inliers while class 1, downsampled to 10 instances, is the outlier class.

6 Complexity of CHAODA

Here we provide short proofs for the time complexity and space complexity of the CHAODA algorithms. For each algorithm, we have a dataset X with n=|X| points and a graph G(V,E) of clusters/vertices V and edges E between overlapping clusters.

6.1 CLAM Clustering

We use CLAM to build the cluster-tree and the induced graphs. The time complexity of clustering is the same as for clustering in CHESS [16]; i.e., expected $\mathcal{O}(nlogn)$ and worst-case $\mathcal{O}(n^2)$ where n is the size of the dataset.

The cost for inducing graphs depends on whether it is a layer-graph or an optimal graph. For both types of graphs, we first have to select the right clusters, and then find neighbors based on cluster overlap.

Table S2: Datasets used for Benchmarks

| Dataset | ble S2: Dataset Cardinality | # Dim. | # Outliers | % Outliers |
|-------------|-----------------------------|--------|------------|------------|
| annthyroid | 7,200 | 6 | 534 | 7.42 |
| arrhythmia | 452 | 274 | 66 | 15 |
| breastw | 683 | 9 | 239 | 35 |
| cardio | 1,831 | 21 | 176 | 9.6 |
| cover | 286,048 | 10 | 2,747 | 0.9 |
| glass | 214 | 9 | 9 | 4.2 |
| http | 567,479 | 4 | 2,211 | 0.4 |
| ionosphere | 351 | 33 | 126 | 36 |
| lympho | 148 | 18 | 6 | 4.1 |
| mammography | 11,183 | 6 | 260 | 2.32 |
| mnist | 7603 | 100 | 700 | 9.2 |
| musk | 3,062 | 166 | 97 | 3.2 |
| optdigits | 5,216 | 64 | 150 | 3 |
| pendigits | 6,870 | 16 | 156 | 2.27 |
| pima | 768 | 8 | 268 | 35 |
| satellite | 6,435 | 36 | 2036 | 32 |
| satimage-2 | 5,803 | 36 | 71 | 1.2 |
| shuttle | 59,097 | 9 | 3,511 | 7 |
| smtp | 95,156 | 3 | 30 | 0.03 |
| thyroid | 3,772 | 6 | 93 | 2.5 |
| vertebral | 240 | 6 | 30 | 12.5 |
| vowels | 1,456 | 12 | 50 | 3.4 |
| wbc | 278 | 30 | 21 | 5.6 |
| wine | 129 | 13 | 10 | 7.7 |

We implemented CLAM in Python and the language does not have tail-call optimization for recursive functions. Therefore we implement partition to, instead of recursing until reaching leaves, iteratively increase the depth of the tree. During the course of this partition, we store a map from tree-depth to a set of clusters at that depth. Therefore, selecting all cluster at a given depth costs $\mathcal{O}(1)$ time and $\mathcal{O}(|V|)$ space where V is the set of selected clusters. Selecting clusters for optimal-graphs is more expensive. First, we use a trained meta-ml model to predict the AUC contribution from each cluster in a tree; this costs $\mathcal{O}(n)$ time and $\mathcal{O}(n)$ space. Next, we sort the clusters by this predicted value; this costs $\mathcal{O}(nlogn)$ time and $\mathcal{O}(n)$ space. Finally, we perform a linear pass over the clusters to select the best for the graph, while discarding the ancestors and descendants of any cluster that has already been selected; this costs $\mathcal{O}(n)$ time and $\mathcal{O}(|V|)$ space. Therefore, the total cost of selecting clusters for optimal graphs is $\mathcal{O}(nlogn)$ time and $\mathcal{O}(n)$ space.

Once the clusters have been selected for a graph, we have to find every pair of clusters with overlapping volumes. Naïvely, this can be done with an all-pairs distance computation for a cost of $\mathcal{O}(|V|^2)$ and $\mathcal{O}(|V|^2)$. However, our implementation is superior to the naïve method although the proof is beyond the scope of this supplement.

6.2 Relative Cluster Cardinality

This algorithm performs a single linear pass over the vertices in the graph. The cardinalities of clusters are cached during the tree-building phase of clam. Each lookup from this cache costs $\mathcal{O}(1)$. For a graph G(V,E) the time-complexity is trivially $\mathcal{O}(|V|)$. Since each cluster stores its cardinality, the space complexity is also $\mathcal{O}(|V|)$.

6.3 Relative Component Cardinality

This method first finds the components of the graph. This costs $\mathcal{O}(|E|)$ time because we have to check each edge once. The cardinality of each component is cached when traversing the clusters to find components, thus the space complexity

is $\mathcal{O}(|C|)$ where C is the set of distinct connected components in the graph. With this done, the algorithm performs a single linear pass over each component. This brings the total worst-case cost to $\mathcal{O}(|E| + |V|)$.

6.4 Graph Neighborhood

This algorithm performs a linear pass over the clusters in the graph and first computes the eccentricity of each cluster. Finding the eccentricity of a vertex in a graph is worst-case $\mathcal{O}(|E|)$ time when the graph consists of a single component. This brings the total cost up to $\mathcal{O}(|E| \cdot |V|)$, with space complexity $\mathcal{O}(|V| + |E|)$. Next, the algorithm performs a traversal from each cluster. This adds a constant factor of $\mathcal{O}(|E|)$ to the time complexity and $\mathcal{O}(|V|)$ to the space complexity, which can be ignored. The total time-complexity of this algorithm is thus $\mathcal{O}(|E| \cdot |V|)$ and its space complexity is $\mathcal{O}(|V|)$ (because only the size of each graph-neighborhood needs to be stored).

6.5 Child-Parent Cardinality Ratio

While building the tree with CLAM, we cache the child-parent cardinality ratios of every cluster, because it proved useful for purposes other than anomaly detection. This method performs a single linear pass over the clusters in the graph and looks-up the cached child-parent ratios as needed. The time-complexity is thus $\mathcal{O}(|V|)$. Since the ratios are cached with their respective clusters, the space complexity is $\mathcal{O}(|V|)$.

6.6 Random Walks

This method is dominated by the computation of a transition matrix for each component in the graph. We set the transition probability from a cluster to a neighbor to be inversely proportional to the distance between their centers, normalized by all possible neighbors of the cluster. In the worst-case, the graph contains only one component, so the time-complexity is $\mathcal{O}(|V|^2)$. The remainder of the algorithm performs a random with with a relatively large number of steps. We used $10 \cdot |V|$ steps in our implementation. Thus the time-complexity stays at $\mathcal{O}(|V|^2)$. In terms of space, we need to store the transition matrix, and the visitation count for each cluster. Therefore the space complexity is $\mathcal{O}(|V|^2)$.

In practice, $|V| \ll n$ and graphs only rarely consist of only one component. Thus, the average run-time performance is much better than that suggested by the quadratic space time-complexity.

6.7 Stationary Probabilities

Just as with Random Walks, this method starts by computing a transition matrix for each component in the graph. We then successively square this matrix until it converges. The transition matrices from our graphs obey the criteria required for convergence as proven in [21]. Matrix multiplication for square matrices costs $\mathcal{O}(|V|^{2.373})$ with the Coppersmith-Winograd algorithm [6]. Thus the worst-case time complexity is the same as that for the matrix-multiplication algorithm employed. For space, we need only store a single $|V| \times |V|$ matrix, giving us a space complexity of $\mathcal{O}(|V|^2)$.

Also just as with Random Walks, because $|V| \ll n$ and graphs only rarely consist of only one component, the average-case run-time performance is much better.

6.8 Normalization

Normalizing the outlier scores requires finding the mean and standard deviation of the raw scores, followed by a linear pass over the set of scores. Thus the time-complexity of this step is $\mathcal{O}(n)$. Since we need to store a score for each point, the space complexity is $\mathcal{O}(n)$.

6.9 Ensemble

Given the normalized scores from the individual methods, we combine the scores by voting among them in an ensemble. There is a small, constant, number of scores for each point; each score is from a different graph built using the meta-ml models. We simply take the mean of all scores for each point. Thus the time-complexity of voting among these scores is $\mathcal{O}(n)$ for the entire dataset. Since we need to store a score for each point, the space complexity is $\mathcal{O}(n)$.

7 UMAP Visualization

A visualization in Figure S2 using UMAP illustrates a handful of different examples; the anomalies in the Cardio and OptDigits datasets, where CHAODA outperforms other methods, appear to be at the edges of a complex manifold

Table S3: Time taken, in seconds, on the first half of the Test Datasets

| Model | Arrhy | BreastW | Cardio | Cover | Glass | Http | Iono | Lympho | Mammo |
|-------------|--------|---------|--------|--------|-------|--------|--------|--------|--------|
| CHAODA-fast | 6.70 | 4.71 | 135.17 | 1e3 | 1.06 | 119.14 | 2.64 | 1.08 | 46.42 |
| CHAODA | 6.90 | 4.80 | 143.31 | 3e3 | 1.10 | 221.81 | 2.78 | 1.74 | 71.54 |
| ABOD | 0.34 | 0.20 | 0.72 | 24.02 | 0.07 | 19.08 | 0.13 | 0.05 | 3.82 |
| AutoEncoder | 8.00 | 6.18 | 9.05 | 183.70 | 3.99 | 154.20 | 4.99 | 3.79 | 35.26 |
| CBLOF | 0.16 | 0.13 | 0.17 | EX | 0.06 | EX | 0.07 | 0.05 | 0.20 |
| COF | 1.24 | 1.84 | 12.63 | 2e4 | 0.24 | 2e5 | 0.60 | 0.14 | 513.46 |
| HBOS | 0.08 | 0.00 | 0.01 | 1.13 | 0.00 | 0.01 | 0.01 | 0.01 | 0.01 |
| IFOREST | 0.43 | 0.34 | 0.43 | 4.61 | 0.30 | 3.95 | 0.33 | 0.30 | 0.95 |
| KNN | 0.19 | 0.07 | 0.30 | 11.46 | 0.02 | 7.47 | 0.05 | 0.02 | 1.58 |
| LMDD | 14.85 | 2.62 | 22.12 | 1e4 | 0.57 | 4e3 | 1.73 | 0.42 | 243.01 |
| LOCI | 307.04 | TO | TO | TO | 25.68 | TO | 120.92 | 9.78 | TO |
| LODA | 0.04 | 0.03 | 0.05 | 0.81 | 0.03 | 0.66 | 0.03 | 0.03 | 0.17 |
| LOF | 0.16 | 0.01 | 0.18 | 10.24 | 0.00 | 1.93 | 0.01 | 0.00 | 0.59 |
| MCD | 5.08 | 0.64 | 0.89 | 28.65 | 0.05 | 8.21 | 0.15 | 0.05 | 2.11 |
| MOGAAL | 46.46 | 42.09 | 116.73 | TO | 40.67 | TO | 40.86 | 37.84 | TO |
| OCSVM | 0.10 | 0.02 | 0.23 | 257.95 | 0.00 | 257.28 | 0.01 | 0.00 | 6.37 |
| SOD | 1.19 | 1.89 | 13.39 | TO | 0.31 | TO | 0.76 | 0.20 | 521.25 |
| SOGAAL | 6.70 | 5.03 | 14.43 | 591.14 | 3.95 | 597.17 | 4.71 | 3.96 | 92.27 |
| SOS | 0.69 | 47.40 | 4.11 | TO | 0.18 | TO | 0.33 | 0.11 | TO |
| VAE | 10.00 | 7.75 | 10.89 | 223.09 | 5.27 | 175.59 | 6.66 | 5.21 | 40.87 |

(though, clearly, the UMAP projection has distorted the manifold). In the Mnist dataset, where several methods perform fairly well, the distribution is less interesting. Most anomalies are off to one side but there are several interspersed among the inliers.

In Figure S3, we show UMAP visualizations of the Pima dataset. The inliers and outliers seem inseparable, and so all the methods perform poorly.

8 Performance

8.1 Run-time performance on Test set of Datasets

Tables S3 and S4 report the running time, in seconds, of CHAODA and each competitor. The fastest methods on each dataset are presented in bold face.

8.2 AUC and Runtime performance on Train set of Datasets

Tables S5 and S6 report the the AUC performance and running time, respectively, of CHAODA and each competitor on the train set of datasets.

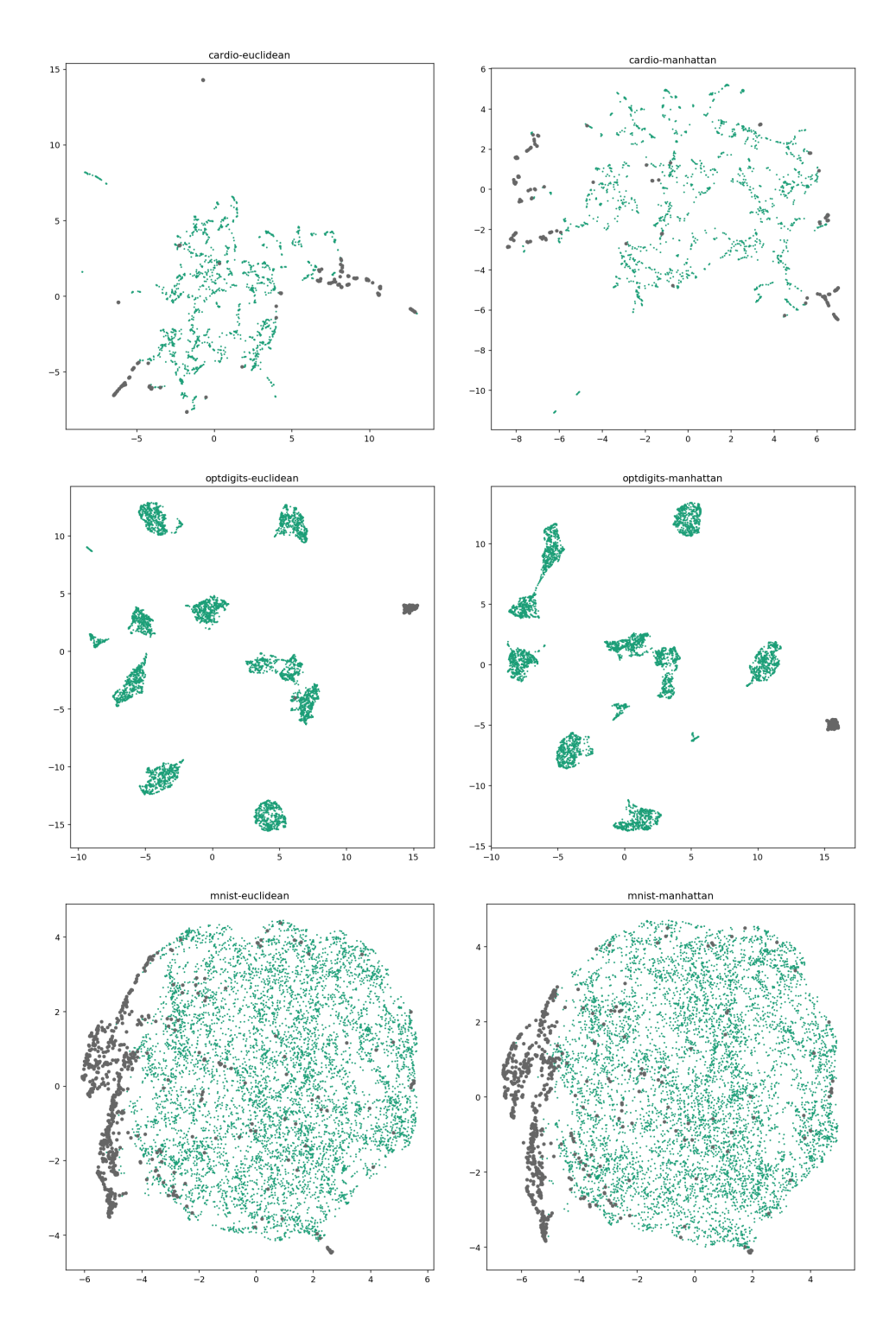


Figure S2: UMAP projections of Cardio (first row), Optdigits (second row) and Mnist (third row). The distance metrics used are Euclidean (left column) and Manhattan (right column). Anomalies are in gray. Note that for MNIST, the UMAP projection does not find much structure, though most of the anomalies congregate to one side. For Cardio, there is a single main component to the manifold, and anomalies tend to be at the edges of that manifold. For OptDigits, there are several distinct pieces to the manifold, perhaps corresponding to different digits. Most algorithms perform comparably on MNIST, while CHAODA outperforms others on Cardio and OptDigits.

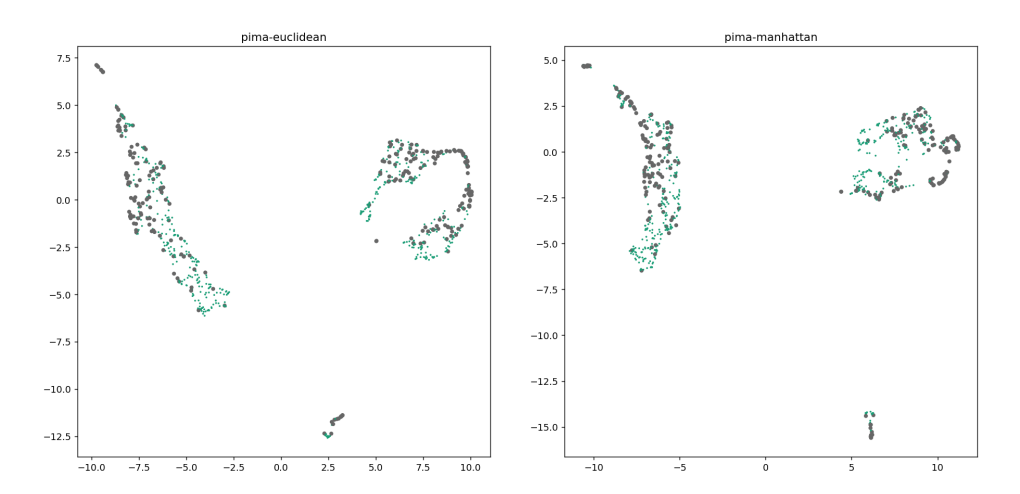


Figure S3: UMAP projections of the Pima dataset. All algorithms performed poorly on Pima. This may be because the anomalies and the outliers seem inseparable in the projection.

Table S4: Time taken, in seconds, on the second half of the Test Datasets

| Model | Must | OptDigits | Pima | SatImg-2 | Smtp | Vert | Vowels | WBC | Wine |
|-------------|--------|-----------|-------|----------|--------|-------|--------|--------|-------|
| CHAODA-fast | 858.15 | 3e3 | 12.36 | 358.49 | 272.61 | 1.88 | 123.34 | 5.26 | 0.39 |
| CHAODA | 982.25 | 6e3 | 13.50 | 611.14 | 451.74 | 2.21 | 181.91 | 6.10 | 0.40 |
| ABOD | 4.39 | 6.81 | 0.26 | 3.20 | 18.00 | 0.08 | 0.51 | 0.14 | 0.04 |
| AutoEncoder | 23.40 | 24.29 | 4.65 | 23.73 | 195.61 | 2.85 | 6.98 | 4.70 | 3.31 |
| CBLOF | 0.27 | 0.44 | 0.08 | 0.31 | 0.65 | 0.06 | 0.10 | 0.08 | 0.05 |
| COF | 45.60 | 119.57 | 2.40 | 141.84 | 2e4 | 0.28 | 8.06 | 0.68 | 0.11 |
| HBOS | 0.07 | 0.04 | 0.00 | 0.02 | 0.01 | 0.00 | 0.01 | 0.01 | 0.00 |
| IFOREST | 0.93 | 0.92 | 0.35 | 0.79 | 3.90 | 0.30 | 0.40 | 0.33 | 0.29 |
| KNN | 3.50 | 5.53 | 0.09 | 1.84 | 6.83 | 0.03 | 0.18 | 0.05 | 0.01 |
| LMDD | 375.11 | 421.22 | 2.86 | 302.94 | 4e3 | 0.59 | 9.47 | 1.91 | 0.33 |
| LOCI | TO | TO | TO | TO | TO | 35.97 | TO | 154.49 | 6.84 |
| LODA | 0.07 | 0.10 | 0.04 | 0.10 | 0.73 | 0.03 | 0.05 | 0.04 | 0.03 |
| LOF | 3.59 | 5.49 | 0.02 | 1.50 | 1.36 | 0.00 | 0.06 | 0.01 | 0.00 |
| MCD | 84.74 | 7.24 | 0.69 | 6.83 | 13.78 | 0.05 | 0.81 | 0.11 | 0.05 |
| MOGAAL | 267.93 | 415.02 | 40.89 | 463.18 | TO | 39.86 | 80.35 | 40.65 | 38.10 |
| OCSVM | 2.51 | 3.71 | 0.03 | 3.14 | 252.52 | 0.00 | 0.11 | 0.01 | 0.00 |
| SOD | 56.94 | 131.49 | 2.48 | 210.39 | TO | 0.54 | 13.92 | 1.03 | 0.19 |
| SOGAAL | 29.55 | 44.72 | 5.20 | 48.79 | 592.27 | 4.69 | 10.38 | 4.76 | 4.01 |
| SOS | 9.37 | 26.09 | 1.01 | 34.96 | TO | 0.21 | 2.81 | 0.36 | 0.10 |
| VAE | 30.38 | 30.58 | 5.67 | 30.41 | 176.84 | 4.03 | 10.46 | 5.33 | 4.62 |

Table S5: Performance on Train Datasets

| Model | Annthy | Mnist | PenDigits | Satellite | Shuttle | Thyroid |
|-------------|--------|-------|-----------|-----------|---------|---------|
| CHAODA-fast | 0.64 | 0.78 | 0.94 | 0.79 | 0.51 | 0.89 |
| CHAODA | 0.65 | 0.73 | 0.95 | 0.73 | 0.85 | 0.89 |
| ABOD | 0.50 | 0.60 | 0.53 | 0.51 | 0.54 | 0.50 |
| AutoEncoder | 0.69 | 0.67 | 0.58 | 0.63 | 0.94 | 0.88 |
| CBLOF | 0.59 | 0.62 | 0.59 | 0.68 | 0.99 | 0.87 |
| COF | 0.59 | 0.56 | 0.53 | 0.56 | 0.52 | 0.49 |
| HBOS | 0.84 | 0.53 | 0.52 | 0.62 | 0.74 | 0.86 |
| IFOREST | 0.70 | 0.61 | 0.63 | 0.70 | 0.91 | 0.91 |
| KNN | 0.65 | 0.65 | 0.51 | 0.56 | 0.53 | 0.56 |
| LMDD | 0.52 | 0.59 | 0.56 | 0.42 | 0.92 | 0.70 |
| LOCI | TO | TO | TO | TO | TO | TO |
| LODA | 0.63 | 0.66 | 0.57 | 0.65 | 0.96 | 0.90 |
| LOF | 0.60 | 0.57 | 0.52 | 0.57 | 0.53 | 0.49 |
| MCD | 0.72 | 0.57 | 0.53 | 0.58 | 0.96 | 0.85 |
| MOGAAL | 0.46 | TO | 0.67 | 0.59 | TO | 0.49 |
| OCSVM | 0.62 | 0.63 | 0.59 | 0.62 | 0.97 | 0.78 |
| SOD | 0.64 | 0.55 | 0.52 | 0.52 | TO | 0.53 |
| SOGAAL | 0.46 | 0.57 | 0.57 | 0.60 | 0.96 | 0.49 |
| SOS | 0.50 | 0.52 | 0.52 | 0.47 | TO | 0.50 |
| VAE | 0.69 | 0.67 | 0.58 | 0.63 | 0.94 | 0.88 |

Table S6: Time taken, in seconds, on Train Datasets

| Model | Annthy | Mnist | PenDigits | Satellite | Shuttle | Thyroid |
|-------------|--------|--------|-----------|-----------|---------|---------|
| CHAODA-fast | 161.85 | 6e3 | 617.93 | 425.03 | 5.48 | 117.97 |
| CHAODA | 205.74 | 1e4 | 771.89 | 891.19 | 2e4 | 219.32 |
| ABOD | 3.42 | 16.39 | 2.83 | 3.53 | 21.58 | 1.25 |
| AutoEncoder | 22.80 | 40.54 | 23.87 | 26.74 | 158.72 | 12.84 |
| CBLOF | 1.01 | 1.14 | 0.23 | 0.30 | 0.71 | 0.21 |
| COF | 215.63 | 277.91 | 199.03 | 176.35 | 1e4 | 54.82 |
| HBOS | 1.58 | 0.06 | 0.01 | 0.02 | 0.03 | 0.00 |
| IFOREST | 0.73 | 1.41 | 0.80 | 0.84 | 3.24 | 0.54 |
| KNN | 0.84 | 14.30 | 1.25 | 2.05 | 9.13 | 0.42 |
| LMDD | 107.05 | 1e3 | 197.48 | 371.63 | 6e3 | 32.69 |
| LOCI | TO | TO | TO | TO | TO | TO |
| LODA | 0.13 | 0.13 | 0.12 | 0.11 | 0.59 | 0.08 |
| LOF | 0.26 | 14.79 | 0.90 | 1.71 | 6.30 | 0.09 |
| MCD | 1.50 | 20.56 | 3.01 | 10.39 | 10.78 | 1.03 |
| MOGAAL | 594.69 | TO | 561.40 | 513.84 | TO | 280.80 |
| OCSVM | 2.70 | 11.30 | 3.04 | 3.83 | 162.18 | 0.68 |
| SOD | 262.80 | 281.86 | 195.81 | 253.71 | TO | 91.48 |
| SOGAAL | 61.14 | 68.03 | 55.40 | 50.07 | 460.66 | 31.43 |
| SOS | 101.82 | 54.22 | 46.02 | 42.62 | TO | 42.10 |
| VAE | 27.95 | 50.16 | 29.63 | 33.51 | 182.23 | 16.18 |